

## RESEARCH ARTICLE

# ClpL is a functionally active tetradecameric AAA+ chaperone, distinct from hexameric/dodecameric ones

Gyuhee Kim<sup>1</sup> | Seong-Gyu Lee<sup>2,3</sup> | Seungsu Han<sup>1</sup> | Jaeun Jung<sup>1</sup> | Hyeong Seop Jeong<sup>4</sup> | Jae-kyung Hyun<sup>4,6</sup> | Dong-Kwon Rhee<sup>5</sup> | Ho Min Kim<sup>2,3</sup> | Sangho Lee<sup>1,7</sup>

<sup>1</sup>Department of Biological Sciences, Sungkyunkwan University, Suwon, Korea

<sup>2</sup>Center for Biomolecular and Cellular Structure, Institute for Basic Science (IBS), Daejeon, Korea

<sup>3</sup>Graduate School of Medical Science and Engineering, Korea Advanced Institute of Science and Technology (KAIST), Daejeon, Korea

<sup>4</sup>Korea Basic Science Institute, Cheongju, Korea

<sup>5</sup>School of Pharmacy, Sungkyunkwan University, Suwon, Korea

<sup>6</sup>Okinawa Institute of Science and Technology Graduate University, Okinawa, Japan

<sup>7</sup>Biomedical Institute for Convergence at SKKU, Sungkyunkwan University, Suwon, Korea

## Correspondence

Ho Min Kim, Center for Biomolecular and Cellular Structure, Institute for Basic Science (IBS), Daejeon 34141, Korea.  
Email: kimhm@ibs.re.kr

Sangho Lee, Department of Biological Sciences, Sungkyunkwan University, Suwon 16419, Korea.  
Email: sangholee@skku.edu

## Present address

Jae-kyung Hyun, Okinawa Institute of Science and Technology Graduate University, Okinawa, Japan

## Funding information

National Research Foundation of Korea (NRF), Grant/Award Number: NRF-2018R1A2B6004367 and NRF-2017R1A5A1014560; Rural Development Agency, Grant/Award Number: PJ01367602; Institute of Basic Science, Grant/Award Number: IBS-R030-C1

## Abstract

AAA+ (ATPases associated with diverse cellular activities) chaperones are involved in a plethora of cellular activities to ensure protein homeostasis. The function of AAA+ chaperones is mostly modulated by their hexameric/dodecameric quaternary structures. Here we report the structural and biochemical characterizations of a tetradecameric AAA+ chaperone, ClpL from *Streptococcus pneumoniae*. ClpL exists as a tetradecamer in solution in the presence of ATP. The cryo-EM structure of ClpL at 4.5 Å resolution reveals a striking tetradecameric arrangement. Solution structures of ClpL derived from small-angle X-ray scattering data suggest that the tetradecameric ClpL could assume a spiral conformation found in active hexameric/dodecameric AAA+ chaperone structures. Vertical positioning of the middle domain accounts for the head-to-head arrangement of two heptameric rings. Biochemical activity assays with site-directed mutagenesis confirmed the critical roles of residues both in the integrity of the tetradecameric arrangement and activities of ClpL. Non-conserved Q321 and R670 are crucial in the heptameric ring assembly of ClpL. These results establish that ClpL is a functionally active tetradecamer, clearly distinct from hexameric/dodecameric AAA+ chaperones.

## KEYWORDS

chaperone, ClpL, Hsp100, *S. pneumoniae*, tetradecamer

**Abbreviations:** AAA+, ATPases associated with diverse cellular activities; AMPNP, adenylyl-imidodiphosphate; aSEC, analytical size-exclusion chromatography; ATP<sub>γ</sub>S, adenosine 5'-O-(3-thiotriphosphate); AUC, analytical ultra-centrifugation; ClpL, caseinolytic protease L; cryo-EM, cryo-electron microscopy; CTD, carboxy-terminal domain; HSP100, heat-shock proteins 100; MD, middle domain; NBD, nucleotide binding domain; NTD, amino-terminal domain; SAXS, small-angle X-ray scattering; SE, sedimentation equilibrium; SV, sedimentation velocity

Gyuhee Kim and Seong-Gyu Lee contributed equally to this study.

## 1 | INTRODUCTION

ATPases associated with diverse cellular activities (AAA+ proteins) are involved in numerous cellular processes, such as membrane fusion, DNA repair, protein homeostasis through coupled proteolysis, and stress adaptation by remodeling protein substrates, to name a few.<sup>1-7</sup> A large number of AAA+ proteins function as chaperones, rendering them essential components in the stress adaptation. Among multiple families of AAA+ chaperones, heat shock protein 100 (HSP100) chaperones prevent unfolded proteins from remaining unfolded or becoming aggregated.<sup>8-10</sup> Three different models for the ATP hydrolysis cycle for ring-shaped, hexameric ATPases have been proposed.<sup>11</sup> In the “synchronized” model, ATP binding and hydrolysis occur simultaneously in all six subunits. In the “rotational” model, every other subunit becomes active in ATP hydrolysis at a time. In the “sequential” model, all subunits are presumably active in ATP hydrolysis with only pairs of subunits being “in phase.”

HSP100 chaperones harbor two nucleotide-binding domains (NBDs) and a middle domain (MD) of variable lengths.<sup>12,13</sup> HSP100 chaperones require hexameric/dodecameric oligomeric states for proper functioning.<sup>1,14,15</sup> Structural and biochemical studies on HSP100 chaperones have demonstrated that HSP100 chaperones operate as hexamer-based oligomers. The crystal structure of ClpA from *E coli* revealed a hexameric assembly.<sup>16</sup> ClpA is associated with ClpP, a protease, serving as degradation machinery.<sup>17</sup> ClpB from *E coli* forms a hexamer or a dodecamer and exhibits disaggregation activity with HSP70 as a co-chaperone.<sup>18,19</sup> Although one case reported a heptameric state of a bacterial ClpB, it was considered to represent an inactive state.<sup>20</sup> Some ClpC chaperones, those from *B subtilis* and *S aureus*, also assemble as hexamers in the presence of an activating cofactor such as MecA, while the dodecameric assembly of ClpC from *S aureus* blocks binding to MecA, thereby representing a “repressed” state.<sup>13,21</sup> It remains unexplored whether non-hexameric oligomers of HSP100 chaperones can be active.

Extensive biochemical and structural studies have suggested that each subunit in the hexameric/dodecameric assembly of an HSP100 chaperone undergoes sequential conformational changes to translocate a substrate polypeptide,<sup>22,23</sup> although some literature report otherwise.<sup>24</sup> As exemplified in structural studies of ClpB and Hsp104, HSP100 chaperones can assume “flat” hexameric states in the absence of a substrate.<sup>13,19,25,26</sup> They subsequently change the assembly to “spiral” conformations so that a substrate polypeptide can be processed along the reaction coordinates during ATP hydrolysis.<sup>27-31</sup> In these steps, the conformation of MD becomes critical in driving changes in the oligomeric assembly of an HSP100 chaperone. In ClpC from *S aureus*, the activating cofactor MecA binding seems to drive the conformational change in the MD. Specifically, the

MD can adopt an equatorial position in the MecA-bound active state and move to a vertical position to become fully inactive in the absence of MecA.<sup>21</sup>

Here, we present the structural and biochemical characterizations of an HSP100 chaperone functioning as a non-hexameric-based oligomer, caseinolytic protease L (ClpL) from *Streptococcus pneumoniae*. Phylogenetically ClpL is related to ClpC, ClpB, and its eukaryotic ortholog Hsp104.<sup>32</sup> Unlike other Clp proteins, ClpL is unique in that it functions as a molecular chaperone without co-chaperones or adaptor proteins.<sup>33</sup> We find that ClpL forms a tetradecamer in solution and that the tetradecameric oligomeric state of ClpL represents a functionally active form.

## 2 | MATERIALS AND METHODS

### 2.1 | Plasmids

Gene encoding ClpL (GenBank accession number: NC\_008533.1) from *S pneumoniae* strain D39 was inserted in parallel GST 2 vector using restriction enzymes *NcoI* and *XhoI* (New England Bio Lab, Ipswich, MA, USA) to encode the glutathione *S*-transferase (GST) fusion protein.<sup>33</sup> Plasmids encoding ClpL-Trap mutant (E193A/E526A) where key glutamates in Walker B motifs were mutated to alanine<sup>34</sup> and other mutants were prepared according to the protocol for Quick-Change site-directed mutagenesis kit (Agilent, Santa Clara, CA, USA). Identities of ClpL-Trap and all other mutants were verified by DNA sequencing.

### 2.2 | Protein expression and purification

Plasmids encoding GST fusion proteins of ClpL variants were transformed into *E coli* Rosetta 2 cells. Cultures were inoculated in 10 mL of LB media (USB Corporation, Cleveland, OH, USA) with 50  $\mu\text{g mL}^{-1}$  ampicillin (Acros Organics, Geel, Belgium) containing the transformed Rosetta 2 cells and incubated at 37°C overnight. Next day, the cultured cells were transferred to 500 mL of LB media with 50  $\mu\text{g mL}^{-1}$  ampicillin. Cells were grown at 37°C until OD<sub>600</sub> reached 0.6-0.8. Protein expression was induced with 0.5 mM isopropyl-1-thio- $\beta$ -D-thiogalactopyranoside (GeneDepot, Karty, TX, USA). The induced cells were further grown at 16°C for 16-18 hours. Cells were harvested by centrifugation at 4000 rpm at 4°C for 15 minutes and subsequently lysed in buffer A (20 mM Tris-HCl pH 7.5, 150 mM KCl, and 1 mM DTT). The lysed cells were sonicated with 2s/2s pulses on a VCX 750 ultrasonic processor (Sonics & Materials Inc, Newtown, CT, USA) and centrifuged at 13 000 rpm at 4°C for 20 minutes. Clarified supernatant containing GST-ClpL was loaded to glutathione-agarose resin (GE Healthcare, Chicago, IL, USA)

pre-equilibrated with the buffer A and incubated for 30 minutes at ambient temperature. ClpL-bound resin was washed with buffer B (20 mM Tris-HCl pH 7.5, 500 mM KCl, and 1 mM DTT). A GST-ClpL protein was eluted with buffer C (50 mM Tris-HCl pH 8.0, 150 mM KCl, 1 mM DTT, and 10 mM reduced glutathione). The GST tag was cleaved by the addition of tobacco etch virus (TEV) protease overnight during dialysis against buffer D (20 mM Tris-HCl pH 7.5, 10 mM KCl, and 1 mM DTT). The cleaved GST tag and histidine-tagged TEV protease were captured using glutathione-agarose (GE Healthcare, Chicago, IL, USA) and Ni-NTA (Qiagen, Hilden, Germany) resins. ClpL was further separated on a Resource Q anion exchange column (GE Healthcare, Chicago, IL, USA) pre-equilibrated with the buffer D. ClpL was eluted using 40–50% 1 M KCl gradient in buffer E (20 mM Tris-HCl pH 7.5, 1 M KCl, and 1 mM DTT). Final purification of ClpL was performed on a Superdex 200 exclusion chromatography column (GE Healthcare, Chicago, IL, USA) pre-equilibrated with buffer F (50 mM HEPES-NaOH pH 7.5, 100 mM KCl, 20 mM  $\text{MgCl}_2$ , and 1 mM DTT). Protein purity was checked by SDS-PAGE. Monomeric ClpL was concentrated in Amicon ultra-15 30 kDa centrifugal filter units (Merck Millipore, Burlington, MA, USA). Protein concentration was determined using the Bradford method. Polydispersity and hydrodynamic radius,  $R_H$ , of the purified ClpL analyzed by dynamic light scattering (DLS) on a DynaPro (Wyatt Technology, Santa Barbara, CA, USA) indicated that the purified ClpL was monodisperse monomer in solution (data not shown).

### 2.3 | Oligomerization

6 mM adenosine triphosphate (ATP) or adenosine 5'-O-(3-thiotriphosphate) ( $\text{ATP}\gamma\text{S}$ ) was added to a solution containing 20  $\mu\text{M}$  ClpL monomer. The resulting solution was incubated for 1 hour with shaking at ambient temperature. After incubation, the resulting solution was centrifuged at 13 000 rpm and 4°C for 30 minutes.  $R_H$  of the ClpL oligomer was analyzed on a DynaPro (Wyatt Technology, Santa Barbara, CA, USA). The ClpL oligomer formed in the presence of ATP was separated on a Superose 6 10/300 analytical size-exclusion chromatography (aSEC) column (GE Healthcare, Chicago, IL, USA) pre-equilibrated with buffer G (50 mM HEPES-NaOH pH 7.5, 100 mM KCl, 20 mM  $\text{MgCl}_2$ , 1 mM DTT, and 6 mM ATP). The purity and concentration of the separated ClpL oligomers were characterized by SDS-PAGE and Bradford method.

### 2.4 | Analytical size-exclusion chromatography

A standard curve was constructed using a high molecular weight gel filtration markers kit (GE Healthcare, Chicago,

IL, USA). About 750  $\mu\text{L}$  of a solution containing ClpL oligomer was loaded to a Superose 6 10/300 column (GE Healthcare, Chicago, IL, USA) pre-equilibrated with the buffer G. Molecular masses of the eluted peaks were estimated based on the standard curve.

### 2.5 | Analytical ultracentrifugation

Analytical ultracentrifugation experiments in both sedimentation velocity (SV) and equilibrium (SE) modes were performed on a ProteomeLab XL-I analytical centrifuge (Beckman Coulter, Brea, CA, USA) equipped with Rayleigh interference optics. In SV experiments, the ClpL-Trap mutant oligomer at 1.5  $\text{mg mL}^{-1}$  in the presence of 6 mM ATP was centrifuged at 30 000 rpm in the buffer G at 10°C. The sedimentation coefficient distributions were obtained using the  $c(s)$  method of *SEDFIT*<sup>35</sup> with  $\bar{v} = 0.7327 \text{ mL g}^{-1}$  which was calculated from the amino acid composition and solvent density = 0.9982  $\text{g mL}^{-1}$ . In SE experiments, the ClpL-Trap mutant oligomer at 0.3  $\text{mg mL}^{-1}$  in the presence of 6 mM ATP was centrifuged at 6 000 rpm three days in the buffer G at 10°C. Data from the SE experiments were processed using *SEDNTERP*<sup>36</sup> with partial specific volume = 0.73  $\text{mL g}^{-1}$ , buffer density = 1.008  $\text{g mL}^{-1}$ , and buffer viscosity = 0.10478.

### 2.6 | Cryo-EM data collection

The purified ClpL-Trap was diluted to a concentration of 0.5  $\text{mg mL}^{-1}$  in the presence of 6 mM  $\text{ATP}\gamma\text{S}$  and ATP. 3  $\mu\text{L}$  of ClpL-Trap: $\text{ATP}\gamma\text{S}$  and 4  $\mu\text{L}$  of ClpL-Trap:ATP were loaded onto Quantifoil Cu R1.2/1.3 holey carbon grid (Quantifoil, Großlobichau, Germany) which had been glow-discharged for 30 seconds using Pelco glow-discharge unit (Ted Pella, Inc, Redding, CA, USA). Grids were blotted for 2.5 seconds (blot force 5) at ~100% humidity and then flash-frozen in liquid ethane using a Vitrobot Mark IV (Thermo Fisher, Waltham, MA, USA). Grids were then transferred to and imaged on a Titan Krios transmission electron microscope IV (Thermo Fisher, Waltham, MA, USA) equipped with a field emission source IV (Thermo Fisher, Waltham, MA, USA) operating at an acceleration voltage of 300 kV. Micrographs were recorded in an automated fashion, using EPU software, on Falcon II direct electron detector IV (Thermo Fisher, Waltham, MA, USA) with a magnification of 47 000 $\times$ , which yielded a pixel size of 1.3973 Å. Dose-fractionated images were recorded for 1.8 seconds with a per-frame exposure time of 60 ms (30 subframes) and a dose of ~33 electrons per Å<sup>2</sup> per second (~2 electrons per Å<sup>2</sup> per frame). The total accumulated dose was ~60  $\text{e}^-/\text{Å}^2$ . Images were recorded with a defocus ranging from -1.8  $\mu\text{m}$  to -3.4  $\mu\text{m}$  for ClpL-Trap: $\text{ATP}\gamma\text{S}$  and -0.5 to -3.9  $\mu\text{m}$  for ClpL-Trap:ATP, respectively.

## 2.7 | Cryo-EM image processing

All image processing was performed in *RELION 2.1*<sup>37</sup> otherwise stated. For each data set, movie frames 2-29 of each image were subjected to drift-correction using *MOTIONCORR2*<sup>38</sup> with dose compensation, and contrast transfer function (CTF) parameters were estimated using *CTFFIND4*.<sup>39</sup> For each data set of ClpL-Trap:ATP $\gamma$ S and ClpL-Trap:ATP, ~2000 particles were manually selected and extracted into 200 × 200 pixel box. These manually selected particles were subjected to reference-free two-dimensional classification to generate two-dimensional references that were used for auto-picking as templates. The total numbers of particles picked for ClpL-Trap:ATP $\gamma$ S and ClpL-Trap:ATP were 377 780 and 252 233, respectively. Following the automated particle selection, 200 × 200 pixel particle images were extracted from the motion-corrected and dose-filtered images. An initial round of reference-free two-dimensional classification and averages were calculated from each data set to remove false positive and defective particles, and those classes that displayed clear secondary-structure detail were taken forward to three-dimensional (3D) classification.

The 280 253 (ClpL-Trap:ATP $\gamma$ S) and 97 906 (ClpL-Trap:ATP) selected particles were subjected to three-dimensional classification procedures. For the initial models, 60 Å low pass-filtered maps obtained from a cylinder (height, 200 Å; diameter, 140 Å) were used. For 3D processing, both dihedral 7 (D7) and cyclic 1 (C1) symmetries were applied. 3D classification split each data set of ClpL-Trap:ATP $\gamma$ S and ClpL-Trap:ATP into four classes. For the ClpL-Trap:ATP $\gamma$ S data set, two of the four 3D classes which appeared similar were recombined to form the final data set (78 587 particles). For the ClpL-Trap:ATP data set, two distinct 3D classes among the similar data set were selected (39 483 particles). These selected ClpL-Trap:ATP $\gamma$ S and ClpL-Trap:ATP data sets were further three-dimensionally refined with D7 and C1 symmetry, respectively. The overall resolutions of tetradecameric ClpL-Trap:ATP $\gamma$ S and ClpL-Trap:ATP were 4.7 and 6.99 Å, respectively. Local resolution estimates were calculated using *BLOCCRES*<sup>40</sup> with the two unbinned and unsharpened half-maps as the inputs. The final data sets were subjected to the “post-processing” in which a soft mask was calculated and applied to the two half-maps before the corrected Fourier shell criterion (FSC) was calculated. Temperature-factor estimation and map sharpening were also performed in the post-processing step using an automated procedure.

To enhance the overall resolution of the cryo-EM maps, we re-processed images using *cisTEM*.<sup>41</sup> We used models processed at 4.7 Å (ClpL-Trap:ATP $\gamma$ S) and 6.99 Å (ClpL-Trap:ATP) as reference models. For each data set, we classified good images using CTF sorting method. After CTF

sorting, we used 262 (ClpL-Trap:ATP $\gamma$ S) and 645 (ClpL-Trap:ATP) micrographs, respectively. About 64 674 (ClpL-Trap:ATP $\gamma$ S) and 104 148 (ClpL-Trap:ATP) particles were picked. About 49 797 (ClpL-Trap:ATP $\gamma$ S) and 52 689 (ClpL-Trap:ATP) particles selected from serial 2D classification were subjected to 3D classification procedures. These selected ClpL:ATP $\gamma$ S and ClpL:ATP data sets were further three-dimensionally refined with D7 symmetry. The final overall resolutions of tetradecameric ClpL:ATP $\gamma$ S and ClpL:ATP maps were 4.5 and 6.33 Å, respectively. The final resolution was estimated using the “gold-standard” FSC = 0.143.

## 2.8 | Model building and refinement

The crystal structure of *Thermus thermophilus* ClpB (PDB 1QVR) was used as a template for initial fitting in ClpL-Trap:ATP $\gamma$ S 4.7 Å and ClpL-Trap:ATP 7.2 Å maps. Enhancement of model building was performed using ClpL-Trap:ATP $\gamma$ S 4.5 Å and ClpL-Trap:ATP 6.3 Å maps. Briefly, the models were initially docked into each cryo-EM density map using *UCSF CHIMERA*<sup>42</sup> and then manually rebuilt in *COOT*<sup>43</sup> to fit the density after visual inspection. Real-space refinement was performed with *PHENIX*.<sup>44</sup> To improve model geometry and backbone placement errors due to near-atomic resolution map, initial models were refined by automated structure refinement based on peptide fragment replacement fit to map by *ROSETTA*.<sup>45</sup> The final model contained residues 76-698 for both ClpL-Trap:ATP $\gamma$ S and ClpL-Trap:ATP complexes.

## 2.9 | Small-angle X-ray scattering

ClpL oligomer samples were concentrated in Amicon ultra-15 100 kDa centrifugal filter units (Merck Millipore, Burlington, MA, USA). Final concentrations were measured by the Bradford assay method. The buffer G was used to record the reference buffer scattering profile. Each sample was measured twelve times and monitored for radiation damage. Samples were serially diluted (two, four, and eight-fold) with the buffer G to check for concentration dependency. Scattering profiles were generated using in-house software at the beamline 4C, Pohang Accelerator Laboratory. Radius of gyration,  $R_g$ , and  $I(0)$  from Guinier plot were calculated using *AUTORG*.<sup>46</sup> *GNOM*<sup>46</sup> was used to calculate the pair distribution function and Porod volume. The experimental scattering profile curve in solution was compared with that of the cryo-EM structure using *CRY SOL*.<sup>47</sup> Ab initio molecular envelope of the tetradecameric ClpL in solution was derived by *DAMMINF*<sup>48</sup> and *DAM AVER*.<sup>49</sup> The derived molecular envelope was refined using *DAMMIN*.<sup>50</sup> Superimpositions between the

cryo-EM structure and ab initio models were performed by SUPCOMB.<sup>51</sup>

## 2.10 | ATPase activity assay

ATPase activity of ClpL was measured by a colorimetric assay<sup>33</sup> with minor modifications. About 1  $\mu$ M ClpL protein in the buffer D was added to buffer H (50 mM Mops-NaOH pH 7.0, 100 mM KCl, 4 mM MgCl<sub>2</sub>, and 4 mM ATP) to make the total volume of 100  $\mu$ L. The reaction mixture was incubated for 20 minutes at 25°C. After 20 minutes, the reaction was terminated by adding 100  $\mu$ L of termination solution (2 mL of 0.082% (w/v) malachite green, 1 mL of 5.72% (w/v) ammonium molybdate in 6 M HCl, 1 mL of 2.32% (w/v) polyvinyl alcohol in hot water). The color change reaction was monitored at 630 nm on an ELx800 microplate reader (BioTek, Winooski, VT, USA). Concentrations of the released phosphate ion were calculated according to a phosphate ion standard curve.

## 2.11 | Holdase/disaggregase activity assay

6  $\mu$ M ClpL protein in buffer I (50 mM HEPES-NaOH pH 7.5, 150 mM KCl, 6 mM MgCl<sub>2</sub>, and 6 mM ATP) was mixed with 1  $\mu$ M native luciferase (Sigma Aldrich, St. Louis, MO, USA) and the resulting solution was incubated for 20 minutes at 25°C. Turbidity was monitored by light scattering at 575 nm at 44°C on a Synergy Neo2 microplate reader (BioTek, Winooski, VT, USA). Detection was made at 30 seconds intervals for 90 minutes. Reaction mixture without ClpL and that without ATP were used as controls.

## 2.12 | Refolding assay

We employed a protocol for refolding assay of a heat-denatured substrate<sup>52</sup> with minor modifications. About 4  $\mu$ M GFP was added to the buffer J (40 mM Tris-HCl pH 7.5, 50 mM KCl, 1 mM DTT, and 8 M urea) and incubated 20 minutes at 85°C. Denatured GFP was 80-fold diluted in ATP regeneration buffer (40 mM Tris-HCl pH 7.5, 50 mM KCl, 10 mM MgCl<sub>2</sub>, 0.015% BSA, 10  $\mu$ g creatine kinase, 10 mM phosphocreatine, and 6 mM ATP). About 6  $\mu$ M ClpL was then added and the reaction mixture incubated for 2 hours at 25°C. Renatured GFP was measured by monitoring fluorescence with excitation at 395 nm and emission at 510 nm on a Synergy Neo2 microplate reader (BioTek, Winooski, VT, USA). Data were normalized by the fluorescence of the native GFP. For the refolding assay of a chemically denatured substrate, 4  $\mu$ M luciferase was added to the buffer J and incubated for 1 hour at 45°C. The

urea-denatured luciferase was then 80-fold diluted in the ATP regeneration buffer. Subsequently, 6  $\mu$ M ClpL was added and the reaction mixture incubated for 90 minutes at 30°C. After incubation, 15  $\mu$ M luciferin (Sigma Aldrich, St. Louis, MO, USA) was added in the refolding sample reaction. Refolded luciferase was measured by monitoring luminescence on a GloMax96 microplate luminometer (Promega, Madison, WI, USA). Data were normalized by the luminescence of the native luciferase.

## 3 | RESULTS

### 3.1 | ClpL exists as a tetradecamer in solution

Previously we reported that ClpL was likely to form hexamers in the presence of ATP based on sequence similarity to ClpB and Hsp104 and size-exclusion chromatograms on an S200 column,<sup>33</sup> which suggested that ClpL might have a hexameric assembly similar to that of ClpA, ClpB, ClpC or Hsp104.<sup>13,19,33,53</sup> However, the retention volume of the oligomeric ClpL peak was close to the void volume, raising the possibility that ClpL may form an oligomer larger than a hexamer. To characterize the oligomeric state of ClpL in solution further, we performed size-exclusion chromatography on a Superose 6 column having a broader molecular mass range. The retention volume of the oligomeric peak of ClpL appeared earlier than that of hexameric ClpB, suggesting that ClpL was not hexameric in solution (Figure 1A). The calibration curve using standards with known molecular masses suggested the molecular mass of ClpL being close to 1 MDa (molecular mass of ClpL monomer is 78 kDa), exceeding that of a hexameric assembly. Initially, we interpreted that ClpL may form a dodecamer, which would be consistent with the oligomeric states of other members in HSP100 family such as ClpB and ClpC.<sup>13,19,26,54</sup> The active site “trap” mutant E193A/E526A in which two residues in the Walker B motifs of two NBDs (E193A/E526A) were mutated (hereafter ClpL-Trap) and reported to slow down ATP hydrolysis<sup>34</sup> also exhibited the same elution profile in size-exclusion chromatography (Figure 1B). To accurately determine the oligomeric state of ClpL, we pursued analytical ultracentrifugation (AUC). Sedimentation velocity data suggested that the molecular mass of ClpL in the presence of ATP in solution is 1.15 MDa (Figure 1C) and interference sedimentation equilibrium data 1.16 MDa (Figure 1D). These results are consistent with the oligomeric state of ClpL being a tetradecamer. To corroborate the oligomeric state of ClpL revealed by the AUC, we took electron micrographs of the oligomeric ClpL in the presence of ATP using negative staining (Figure 1E). Surprisingly, the negatively stained images of ClpL manifested a heptameric arrangement from top views. Taken together, we concluded that ClpL exists predominantly as a tetradecamer in solution.

### 3.2 | Cryo-EM structure of ClpL tetradecamer

ClpL from *S pneumoniae* consists of an N-terminal domain (NTD), two NBDs (NBD1 and NBD2) connected by the MD, and a C-terminal domain (CTD) at the primary

sequence level (Figure 2A). The well-ordered and stable tetradecameric ClpL was generated in the presence of adenosine triphosphate (ATP) or adenosine 5'-O-(3-thiotriphosphate) (ATP $\gamma$ S) by ClpL-Trap (Figure 2A). We determined a cryo-EM structure of ClpL-Trap at near-atomic resolution in the presence of ATP $\gamma$ S (Table 1 and

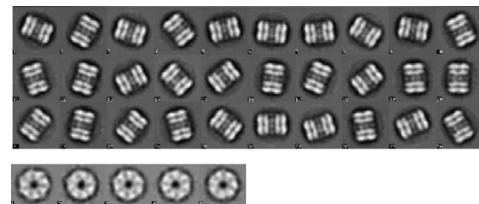
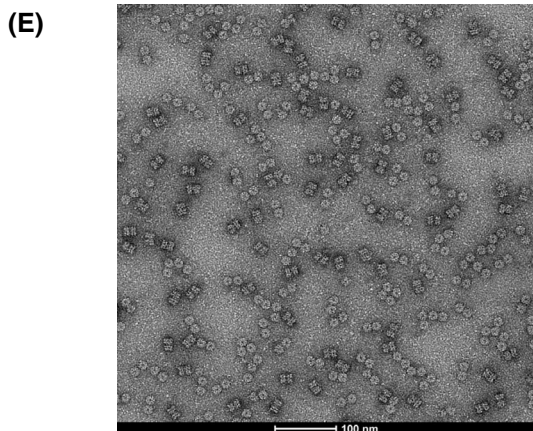
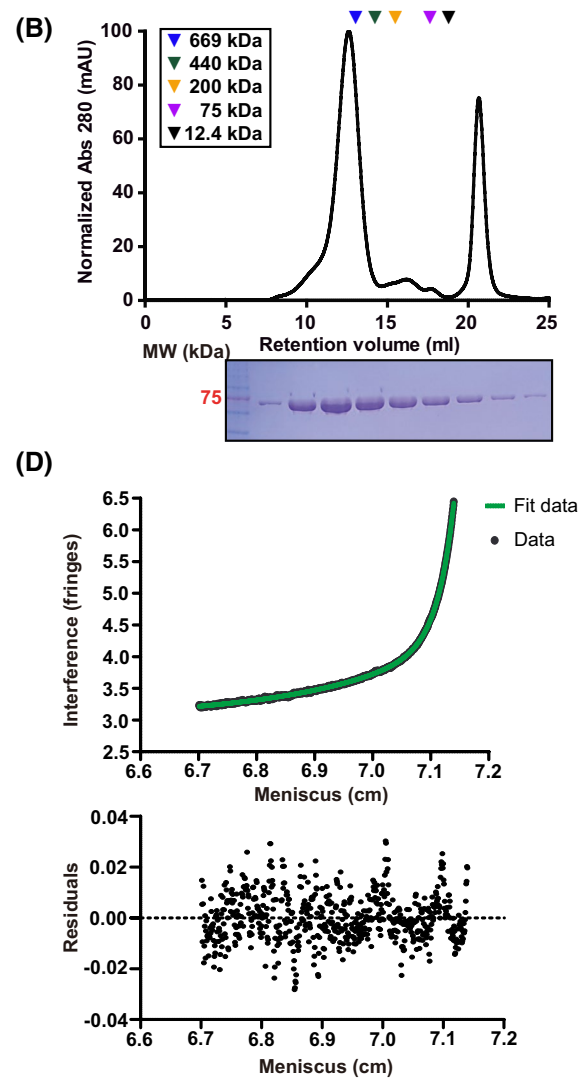
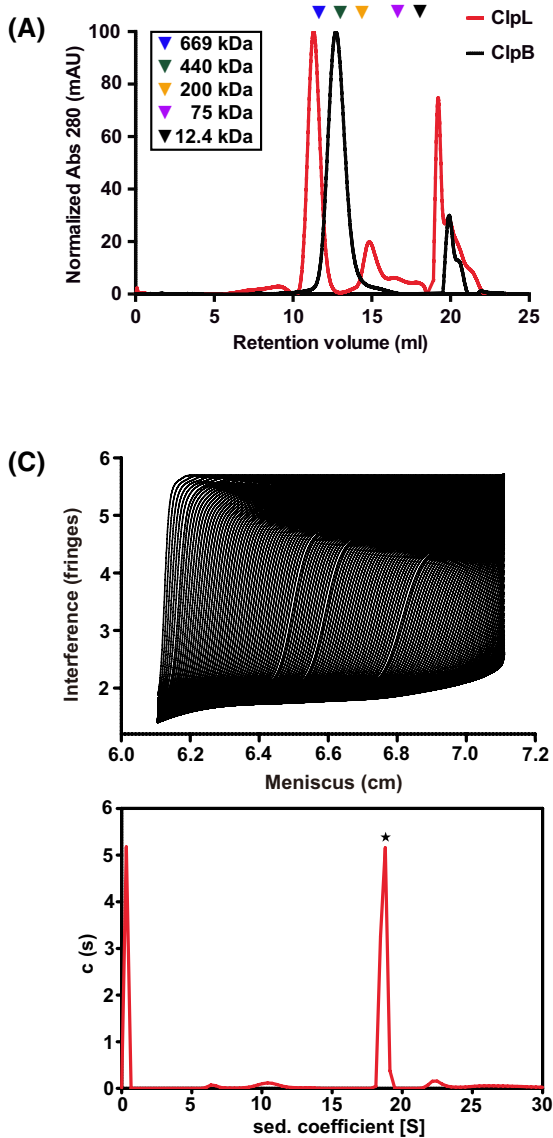


**FIGURE 1** Molecular characterizations of the oligomeric ClpL. A, Analytical size-exclusion chromatograms of ClpL wild-type from *S. pneumoniae* and ClpB from *E. coli*. Proteins were loaded to a Superose 6 column in the presence of 6 mM ATP with molecular mass values of standards indicated above the peaks. B, A chromatogram of ClpL-Trap (E193A/E526A):ATP reveals that the oligomeric state observed in ClpL wild-type is maintained in ClpL-Trap mutant. A Coomassie blue-stained SDS-PAGE gel showing fractions corresponding to the oligomeric ClpL-Trap:ATP is shown at the bottom. C, (Upper) Sedimentation velocity profiles of ClpL-Trap (E193A/E526A) oligomer in solution. Data were acquired on a ProteomeLab XL-I analytical centrifuge (Beckman Coulter) equipped with Rayleigh interference optics. (Lower) Sedimentation coefficient distribution,  $c(s)$ , of ClpL-Trap:ATP obtained by sedimentation velocity experiment is shown. The apparent molecular mass of ClpL-Trap oligomer was estimated to be 1.15 MDa with friction ratio being 2.0. D, Interference sedimentation equilibrium analysis of ClpL-Trap oligomer in solution. Molecular mass of the ClpL-Trap was estimated to be 1.16 MDa, indicating that ClpL-Trap is tetradecamer in solution. E, (Left) A representative image obtained by negative staining on a transmission electron microscope of the tetradecameric ClpL-Trap:ATP (scale bar = 100 nm). 2D averaged images of ClpL-Trap:ATP with side-view (upper right) and top-view (lower right) are shown.

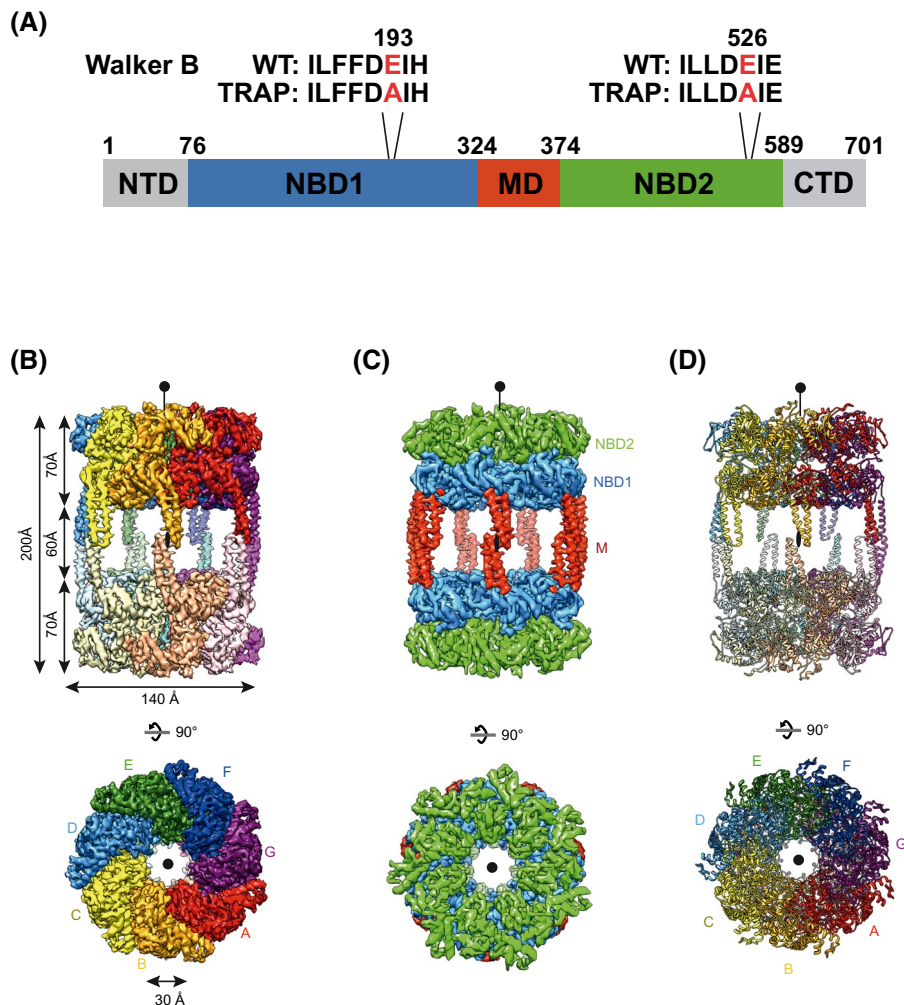


**FIGURE 2** Cryo-EM structure of the tetradecameric ClpL-Trap:ATP $\gamma$ S. A, Domain organization of ClpL is shown with domain boundaries indicated. Domains are described as colored boxes: NTD, N-terminal domain (gray); NBD1, nucleotide-binding domain 1 (blue); MD, middle domain (red); NBD2, nucleotide-binding domain 2 (green); and CTD, C-terminal domain (gray). Residues mutated in the ClpL-Trap mutant are indicated at the top. B, Cryo-EM map of the tetradecameric ClpL-Trap:ATP $\gamma$ S complex at an overall resolution of 4.5 Å. Side-view (upper) and top-view (lower) are provided. Maps are segmented and colored by protomers. Dimensions for the width of the full-length protein, heights of the full-length, each heptameric ring, and MD are shown(upper). ClpL oligomer inner diameter was shown in top-view (lower). C, The same structure as (B) with maps being segmented and colored by domains. The coloring scheme is identical to that in (A). D, Side and top views of the fitted atomic model of tetradecameric ClpL:ATP $\gamma$ S, colored by protomers in cartoon representation.

Figure S1). 2D class average and cryo-EM map from the 3D classification and refinement without imposing any symmetry shows that ClpL-Trap:ATP $\gamma$ S is a tetradecamer

with dual layers each of which is composed of a heptamer at 9.3 Å resolution (Figure S1C-E). To improve the resolution, D7 symmetry was applied for further 3D classification

**TABLE 1** Cryo-EM data collection and processing statistics

	ClpL-Trap:ATP $\gamma$ S (EMDB-0967) (PDB 6LT4)	ClpL-Trap:ATP (EMDB-0965) (PDB 6LSY)
<i>Sample preparation</i>		
Grid	Quantifoil R2/2 200 mesh	
Cryo-specimen freezing	Vitrobot IV	
<i>Data collection</i>		
Electron microscope	Titan krios	
Data collection mode	Electron counting	Linear
Voltage (kV)	300	300
Magnification	47 000	47 000
Pixel size (Å)	1.3973	1.3973
Defocus range ( $\mu$ m)	-1.8 to -3.4	-0.5 to -3.9
Total electron dose (e <sup>-</sup> /Å <sup>2</sup> )	60	60
Exposure time (s)	1.8	1.8
<i>Data processing</i>		
Data processing program	<i>RELION</i> and <i>cisTEM</i>	
Number of micrographs	1164	1821
Number of frames per image	40	30
Initial particle number	63 674	104 148
Final particle number	49 797	52 689
Symmetry imposed	D7	D7
Resolution (Å)	4.5	6.33
<i>Refinement</i>		
Refinement program	<i>PHENIX</i>	
Reference for the initial model	PDB 1QVR ( <i>RELION</i> )	
Reference for the final model	<i>RELION</i> processing model	
<i>Cell dimensions</i>		
<i>a</i> , <i>b</i> , <i>c</i> (Å)	166.28, 166.28, 227.76	164.88, 169.07, 236.14
$\alpha$ , $\beta$ , $\gamma$ (°)	90, 90, 90	90, 90, 90
Map sharpening B-factor (Å <sup>2</sup> )	-388.847	-948.575
<i>Model composition</i>		
Nonhydrogen atoms	68 530	67 662
Protein residues	8 722	8 722
Average B-factor (Å <sup>2</sup> )	81.86	72.8
<i>R m.s deviations</i>		
Bond length (Å)	0.007	0.018
Bond angle (°)	0.972	1.875
<i>Ramachandran plot</i>		
Favored (%)	94.52	95.49
Allowed (%)	5.48	3.70
Disallowed (%)	0.00	0.81
<i>Validation</i>		
Clash score*	8.90	1.43
Rotamer outliers (%)	0.19	0
MolProbity score	1.85	1.19
<i>Mask CC</i>		
	0.71	0.71

\*The MolProbity clash score indicates the number of steric overlaps larger than 0.4 Å per 1000 atoms.

and refinement, yielding a cryo-EM map with a global resolution of 4.5 Å (Figure S1E-G).

The overall structure of tetradecameric ClpL-Trap:ATPγS features two parallel, symmetrical and face-to-face heptameric rings with outer diameter 140 Å, inner diameter 30 Å, and height 70 Å, separated by seven bridges with 60 Å gap distance (Figure 2B). The tetradecameric arrangement of ClpL is striking, considering that most AAA+ ATPases are known to form either hexamers or dodecamers. Each heptameric ring is composed of NBD2 stacked on top of NBD1 with MDs perpendicularly protruding from NBD1s (Figure 2C).

The identity of a nucleotide in the cryo-EM structure of an AAA+ ATPase is often responsible for different conformations.<sup>22,55-57</sup> Structure of an ADP-bound NBD2 of ClpB from *T. thermophilus* features that pore loop is exposed to the central channel for substrate translocation.<sup>22</sup> An AMPPNP-bound ClpB structure from *M. tuberculosis* adopts an open and asymmetric conformation.<sup>57</sup> To investigate whether ATP, not ATPγS, can lead to different conformations of ClpL, we determined the cryo-EM structure of ClpL-Trap in the presence of ATP at 6.3 Å resolution (Table 1 and Figure S2A-F). No noticeable conformational change was observed between ClpL: ATPγS and ClpL:ATP cryo-EM structures.

The cryo-EM structure of tetradecameric ClpL-Trap reveals a flattened conformation while oligomeric HSP100 chaperones assume a twisted or helical arrangement when they are active.<sup>25,58-60</sup> To resolve this controversy, we investigated the solution structure of ClpL-Trap:ATP using small-angle X-ray scattering (SAXS; Table S1). The radius of gyration ( $R_g$ ) of ClpL by SAXS (78 Å) is slightly smaller than that by cryo-EM (83 Å), corroborating that the overall tetradecameric state is likely to be conserved (Figure S2G). Interestingly,  $D_{max}$  value, the maximal distance between two atoms in a structure, assessed by SAXS (257 Å) is somewhat larger than that by cryo-EM (232 Å), suggesting that ClpL may have a more flexible structure in solution (Figure S2H). Ab initio envelopes for ClpL derived from SAXS data appear to be fitted better with a hypothetical helical ClpL tetradecamer than with cryo-EM structure (Figure S2I). These data implicate that active ClpL may assume a non-flattened conformation. The current cryo-EM structure of ClpL seems to reflect conditions where individual ClpL particles are aligned in a thin vitrified environment.

While densities for NBDs and MD are clearly visible in the cryo-EM map, the density for the NTD was missing in 3D reconstruction (Figure 2C), probably due to its high flexibility in the absence of a substrate a similar observation made in other Clp family structures.<sup>13</sup> Mass spectrometry analysis confirmed the presence of the intact NTD (Figure S3A). A construct lacking NTD, ClpL-ΔNTD, exhibited less flexibility judged by Porod-Debye plot<sup>61</sup> derived from SAXS data (Table S1 and Figure S3B), corroborating that the NTD is

flexible. The locations of the N-termini of NBD1 suggest that this missing NTD might be located near the central chamber (Figure S3C). A size-exclusion chromatogram revealed that ClpL-ΔNTD did not cause a shift in its elution volume, implicating that NTD is dispensable in forming the tetradecameric arrangement of ClpL (Figure S3D).

The model built in cryo-EM density map of ClpL revealed that the NBD1 and NBD2 shows a typical AAA+ ATPase fold consisting of a large RecA-like  $\alpha/\beta$  and small  $\alpha$ -helical ATPase subdomain and that the helix-turn-helix of MD forms a coiled-coil structure which protrudes from the small subdomain of NBD1 (Figure 2D and Figure S3C). For both NBDs, the large subdomains are organized as a  $\beta$ -sheet that is flanked by helices on both sides. The small subdomains of NBD1 have a four-helix bundle, while the fourth helix was replaced by the two-stranded  $\beta$ -sheet in the small subdomain of NBD2 (Figure S3C).

The overall subdomain organization and fold of the ClpL protomer is similar to that of the other Clp family proteins, resulting root-mean-square-deviation (r.m.s.d.) 2.1 Å when superimposed with ClpC, a phylogenetically close ortholog (Figure S4A). In the current cryo-EM structure of ClpL-Trap, densities of ATPγS molecules are visible. In NBD1, ATPγS is accommodated in a pocket formed by residues of the Walker A (K127 and T128) and Walker B (D192 and E193) motifs as well as by those of sensor-1 (T231) and sensor-2 (R301) (Figure S4B). In addition, arginine finger from the neighboring protomer (R248\*) protrudes into the ATP binding site, indicating that coordinated inter-protomer communications are also critical for nucleotide sensing and hydrolysis (Figure S4B). In NBD2, the corresponding residues (Walker A: K458, T459; Walker B: D525, E526; sensor-1: N567; sensor-2: R659 and arginine finger: R600) similarly interact with ATPγS (Figure S4C).

The two heptameric rings of ClpL are connected by seven bridges consisting of fourteen vertical MDs (Figure 2D). In the cryo-EM structure, the MDs seem to be an insertion to the NBD1 although the MD is located between NBD1 and NBD2 at the primary structural level. The vertical arrangement of the MDs is also seen in the “repressed” dodecameric ClpC structure.<sup>21</sup> Unlike the dodecameric ClpC structure, however, the tetradecameric ClpL features stacked two heptameric rings, not spiral ones. The region in the MD responsible for the ring-to-ring contact is rather small, burying only 115.8 Å<sup>2</sup>.

### 3.3 | Oligomeric assembly

ClpL is phylogenetically related to other HSP100 proteins such as ClpC, ClpB, and Hsp104 (Figure 3A). Protomers of ClpL-Trap are assembled into a tetradecamer with two-layered heptameric rings, while all the other known HSP100

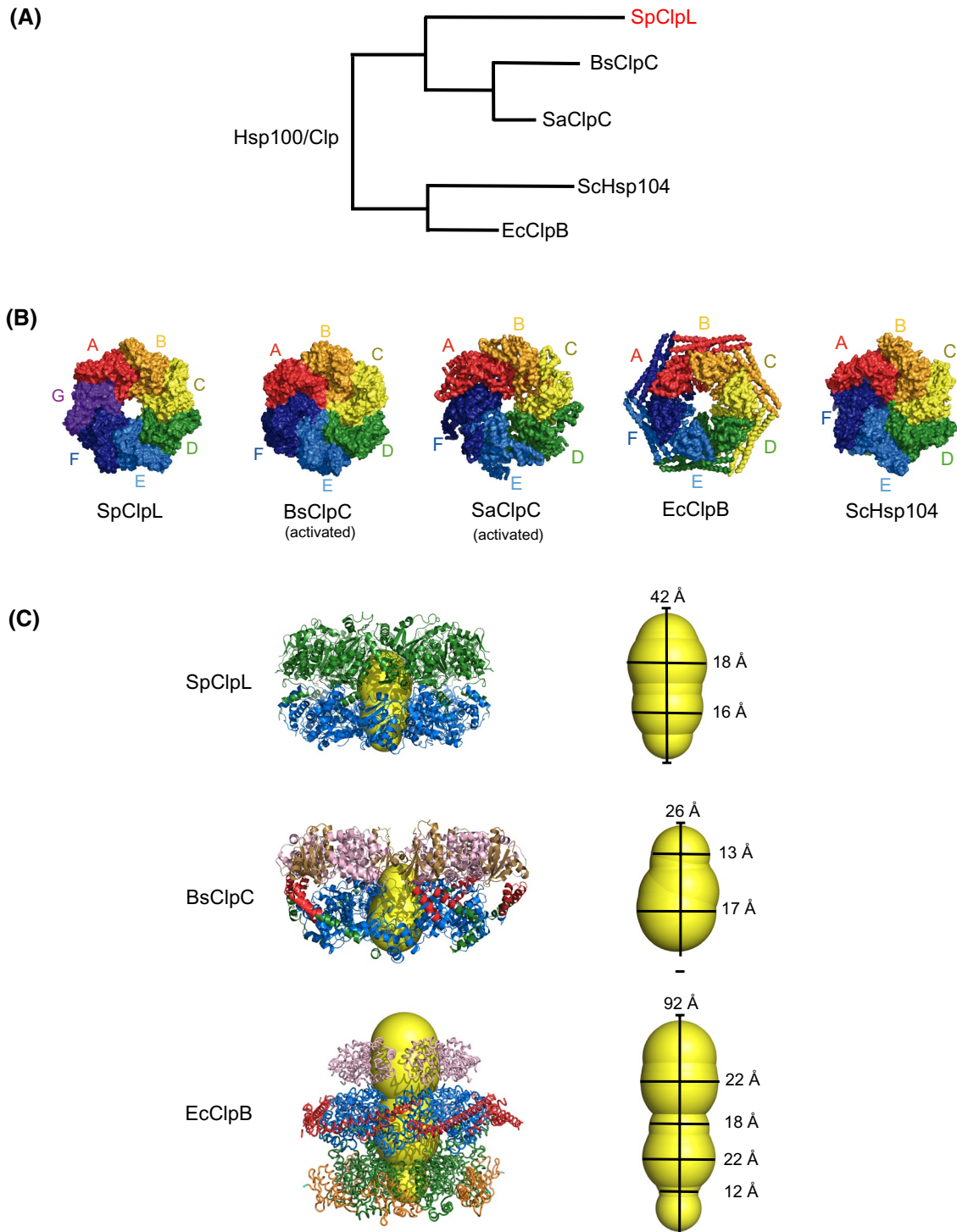


**FIGURE 3** Oligomeric assemblies of ClpL and other HSP100 chaperones. A, Phylogenetic analysis of HSP100/Clp chaperones. SpClpL, ClpL from *Streptococcus pneumoniae*; BsClpC, ClpC from *Bacillus subtilis*; SaClpC, ClpC from *Staphylococcus aureus*; ScHsp104, Hsp104 from *Saccharomyces cerevisiae*; EcClpB, ClpB from *Escherichia coli*. SpClpL is labeled in red. B, ClpL forms a heptameric ring, while other orthologs form hexameric rings. Top-view of oligomers are shown as surface representations. Coordinates used are as follows: SpClpL, this study; BsClpC:MecA complex, PDB ID 3J3U; SaClpC:MecA, PDB ID 6EMW; EcClpB, PDB ID 4D2U; and ScHsp104 closed form, PDB ID 5VJH. Each protomer in an HSP100 chaperone assembly is colored differently. C, Internal chamber volume analysis of SpClpL, BsClpC, and EcClpB. Internal chamber volumes were analyzed by ChExVis.<sup>70</sup> NBD2s of BsClpC form a closed hexameric ring, thereby excluded from calculating the internal chamber volume. Dimensions of the internal chamber volumes are shown in angstrom ( $\text{\AA}$ ). NBD1s (blue) and NBD2s (green) of heptameric ring of SpClpL, NTDs (pink), NBD1s (blue), MDs (red), NBD2 (green) and MecA (olive) of hexameric ring of BsClpC 1-485 and NBD1s (blue), NBD2s (green), MDs (red), NTDs (pink) and CTDs (brown) of EcClpB are shown. Internal chamber volumes are depicted as yellow surface presentations.

proteins form either hexamers or dodecamers (Figure 3B). ClpC exists as either a hexamer (complexed with a cofactor)<sup>13</sup> or a dodecamer (repressed conformation).<sup>21</sup> ClpB and its yeast ortholog Hsp104 feature a single hexameric ring despite the variable positions of the MD. To compare the oligomeric assembly of ClpL to those of other related Clp proteins, we analyzed the internal chamber volume of the heptameric and hexameric rings of ClpL, ClpC, and ClpB (Figure 3C). Since the NTD in the ClpL structure is missing, we confined our analysis to one layer of a ring.

The heptameric ring of ClpL shows an internal chamber with 42 Å in height and 16-18 Å in width. In contrast, the hexameric rings of ClpC and ClpB feature internal cavities with 26 Å in height and 13-17 Å in width for ClpC, and 92 Å in height and 12-22 Å in width for ClpB, respectively. ClpC shows widths of the internal chamber comparable to those of ClpL (13-17 vs 16-18 Å), while the height of the internal chamber of ClpC is about half the height of ClpL (26 vs 42 Å). Although ClpC is the closest ortholog of ClpL phylogenetically among HSP100 chaperones whose

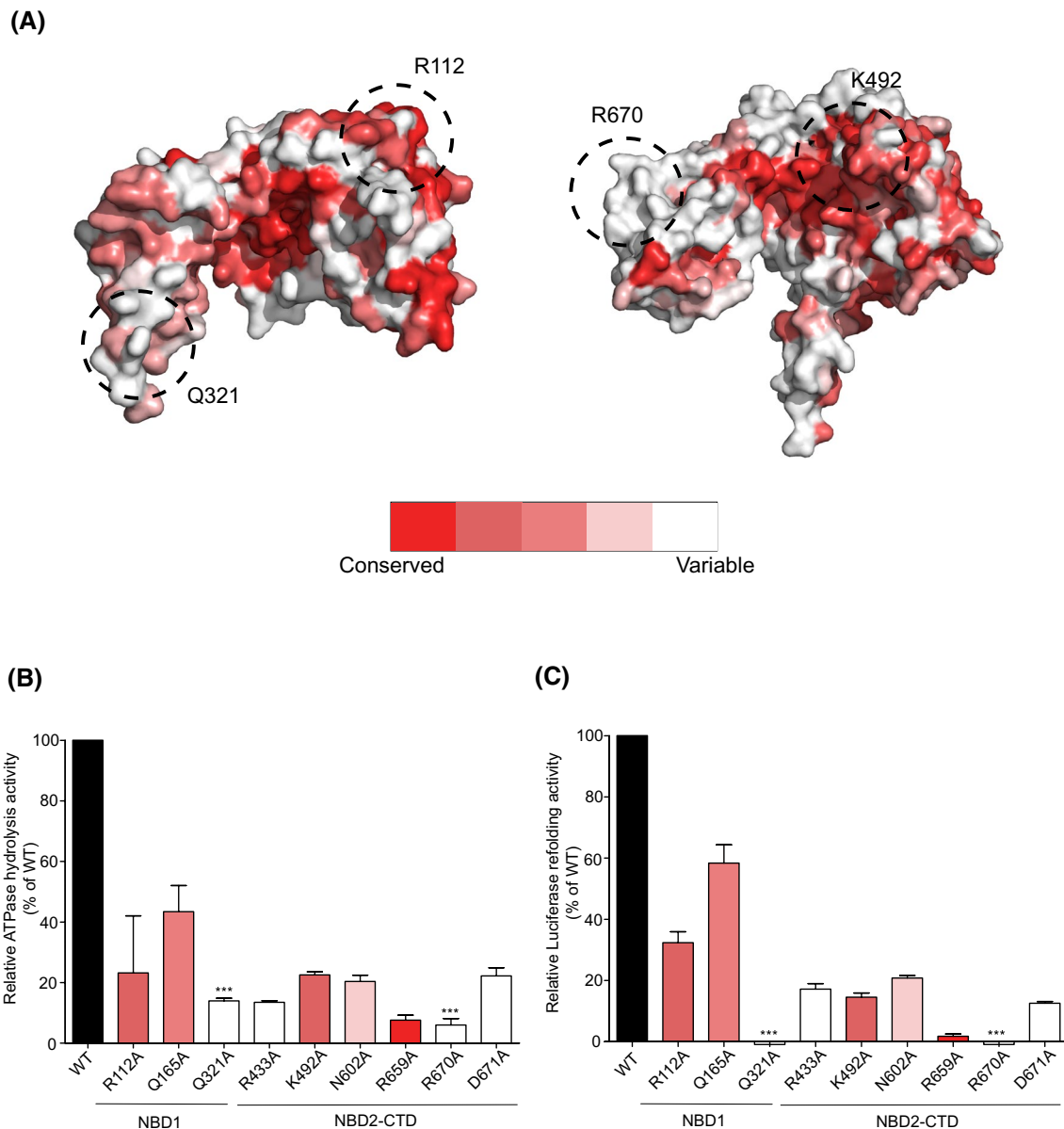


**FIGURE 4** Protomer interface analysis of the heptameric ring of ClpL. A, Conservation analysis of HSP100 chaperones (ClpL, ClpC, ClpB, and Hsp104). Degree of conservation in residues of NBD1 (left) and NBD2 (right) is mapped on surface representations with color varying from red (conserved) to white (variable). The orientations of NBD1 and NBD2 are the same as those in Figure S5A. Key interface residues for hexameric ring assembly (R112 and K492) and those for heptameric ring assembly (Q321 and R670) are labeled. B, C, ATPase activities (B) and refoldase activities (C) of ClpL mutants at the protomer interface. Relative activities of ClpL mutants are shown. Mutants are colored in the same manner in (A) and wild-type (WT) as black. Average and standard deviation values from triplicates are shown. Statistical significance is represented as follows: \*\*\*,  $P \leq .001$ .

structure is well characterized, the internal chamber volume is apparently smaller from that of ClpL. However, ClpC often requires the presence of an adaptor protein such as MecA, which provides an additional open chamber with 23 Å in height and 90 Å in width. At the one-layered ring level, ClpB seems to have a bigger chamber than ClpL: for instance, the height of the internal chamber of ClpB is about two-fold bigger than that of ClpL (92 vs 42 Å). However, considering that ClpL forms two-layered rings one can imagine the total chamber would be comparable to each other. These analyses clearly demonstrate that the oligomeric assembly of ClpL is distinct from those of other HSP100 proteins.

### 3.4 | Protomer arrangement and interfaces

The protomers of the tetradecameric ClpL constitute four kinds of inter-protomer interfaces (Figure S5A): NBD1-NBD1 interface (Figure S5B), MD-NBD1 interface (Figure S5C), NBD2-NBD2 interface (Figure S5D) and CTD-NBD2 interface (Figure S5E). Inter-protomer interactions found in the tetradecameric ClpL share common features with those of other hexameric and dodecameric AAA+ ATPases despite differences in details (Figure S6). R112, K114, and K492 of ClpL are structurally equivalent to residues at the hexameric interface of ClpB (Figure S6A). In contrast, Q165 and Q321 in NBD1, R433 in NBD2, and N602, R659, R670, and D671 in CTD are residues specifically found in the heptameric interface (Figure S6B).

To obtain insights into determinants for the heptameric assembly of ClpL, we analyzed relationship between sequence conservation and the locations of interface residues (Figure 4). Sequence conservation mapped to the structures of NBD1 and NBD2 of ClpL revealed that Q321, a key residue in the NBD1 interface, and R670, one in the NBD2 interface, are located in the non-conserved region (Figure 4A). In contrast, interface residues of hexameric ClpC and ClpB are highly conserved. It appears that the non-conserved residues in ClpL may be responsible for the heptameric ring arrangement of ClpL. To validate functional roles of residues in the heptameric interface, we performed the following activity assays: ATPase and refoldase assays. Virtually all mutations in the heptameric interface residues impaired ATPase hydrolysis whether they are structurally equivalent to residues in hexameric interfaces of other HSP100 proteins or not (Figure 4B), suggesting that the integrity of the heptameric ring is critical in conferring ATPase activity. Interestingly, the refoldase activity of the tetradecameric ClpL was compromised most drastically by residues specific to the heptameric interface such as Q321 in NBD1 and R670 in CTD (Figure 4C). These

results demonstrate that the heptameric interface appears to be more critical in conferring refoldase activity.

To compare the roles of interface residues in heptameric ClpL ring with those of interface residues in hexameric ClpC and ClpB rings, we analyzed locations of the residues in the protomer interface and the MDs of ClpL, ClpC, and ClpB (Figure S7). We chose one residue per each NBD at the protomer interface (Q321 for NBD1 and R670 for NBD2 in ClpL; R405 for NBD1 and R767 for NBD2 in ClpC; and R196 for NBD1 and Q703 for NBD2 in ClpB) and one residue essential for contacts among the MDs (F350 for ClpL, F436 for ClpC and Y503 for ClpB). Then we measured the angle among the three residues (one in the NBD1 interface, one in the NBD2 interface, and one in the MD interface) from the top view. In ClpL, the NBD1 interface residue is rotated clockwise to the NBD2 interface residue by 15° in a protomer (Figure S7A). In contrast, in both ClpC and ClpB, the NBD1 interface residues are rotated counter-clockwise to the NBD2 interface residues by 26° and 24°, respectively (Figure S7B and C). The NBD1 interface residue of ClpL is again rotated clockwise to the MD interface residue by 5° (Figure S7A), while the NBD1 interface residues of ClpC and ClpB are rotated counter-clockwise to the MD interface residues by 8° and 12°, respectively (Figure S7B and C). It seems that the NBD1 interface residue in the tetradecameric ClpL is positioned so that the NBD1 interface residue is rotated clockwise to the NBD2 and MD interface residues, unlike hexameric ClpC and ClpB where the NBD1 interface residues are rotated counter-clockwise to the NBD2 and MD interface residues.

### 3.5 | Vertical arrangement of the middle domains

Structural analysis points out that F350 is a key residue in maintaining the two heptameric rings through MDs (Figures S8A and 5A). The head-to-head interactions between MDs are composed of the three pairs of proximally located hydrophobic residues encompassing V345, F350, A353 and L354 and two pairs of polar residues including E348 and K357 at the tip of the MDs, leading to a stable and rigid tetradecameric ClpL (Figures S8A and 5A). To corroborate the roles of residues at the protomer interface, we compared the oligomeric state of a deletion mutant ( $\Delta$ 339-356) with that of WT by size-exclusion chromatography (Figure 5B). The deletion mutant eluted at about half the size of the WT, confirming the roles of the aforementioned residues in maintaining the tetradecameric state. Furthermore, mutations of the key hydrophobic residue (F350A, F350E, F350R, and D349A/F350A/E351A) also led to the disruption of the tetradecameric state (Figure S8B-E). Superposition of MDs from HSP100

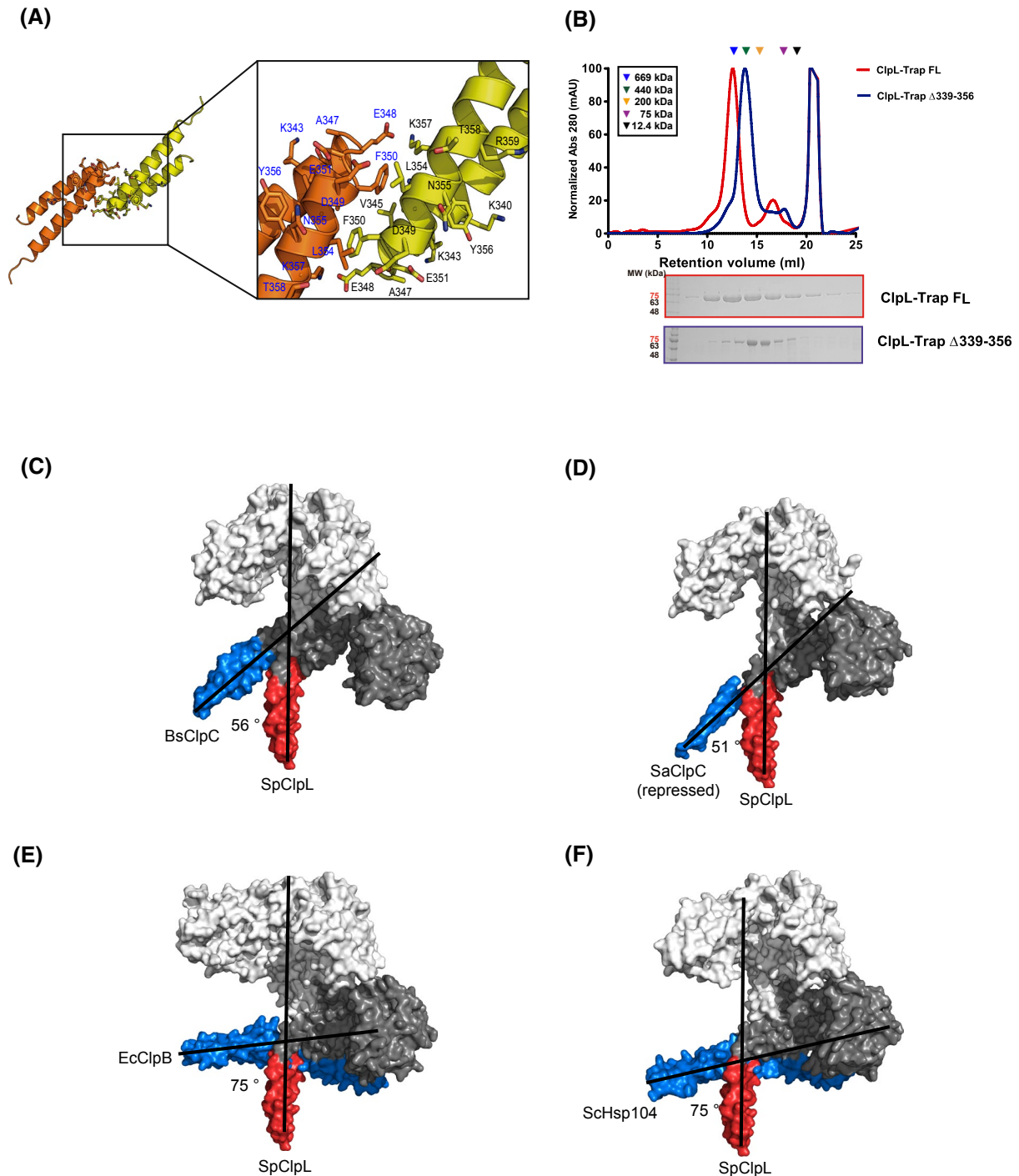


**FIGURE 5** Analysis of MDs of ClpL and its orthologs. A, Close-up of inter-ring interactions between two heptameric rings in a head-to-head manner. Two MDs making inter-ring contacts are shown as ribbon representations with key residues involved in inter-ring contacts as stick models. B, Analytical size-exclusion chromatograms of ClpL-Trap full-length (red) and ClpL-Trap  $\Delta 339-356$  lacking MD residues (blue). 6 mM ATP was added to the protein solution to promote ClpL oligomer formation. Fractions corresponding to the ClpL oligomer peaks were analyzed by SDS-PAGE. C-F, Angle between the MD of ClpL and the MDs of active ClpC (C), repressed ClpC (D), ClpB (E), and Hsp104 (F). The MDs are aligned in reference to the NBD1s (gray). The MD of ClpL is colored as red and the MDs of ClpC, ClpB, and Hsp104 as blue.

family proteins such as ClpB, ClpC, and Hsp104 reveals that subtle rotameric changes contribute to the protomer interface (Figure S8F). This is in contrast to the repressed ClpC oligomer where the ring-to-ring contact is mediated

by hydrogen bonds between E435 and N438.<sup>21</sup> F350 of ClpL, corresponding to F436 of ClpC, assumes a slightly different rotameric position. Such a subtle rotameric difference appears to be crucial in mediating different positioning

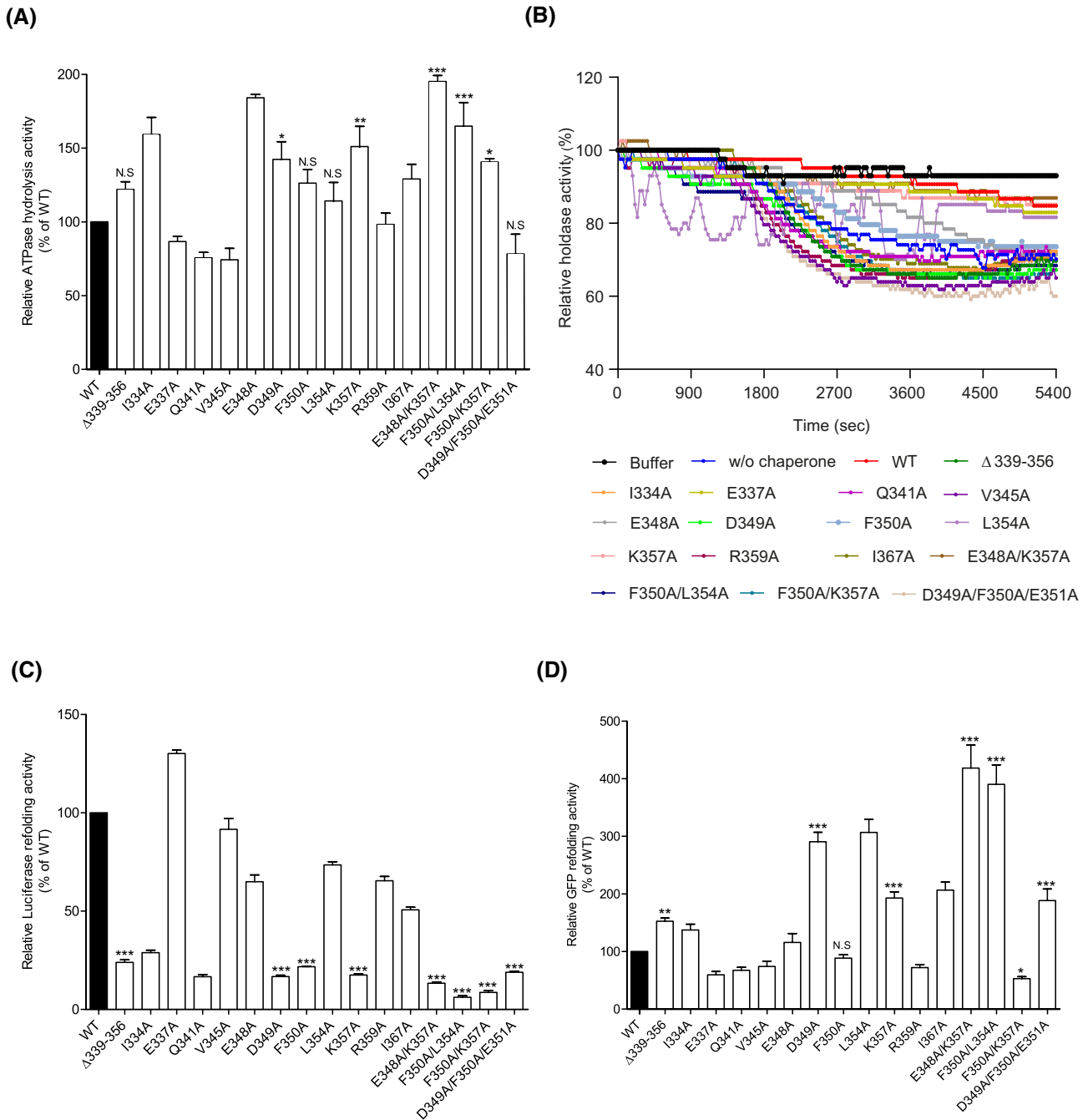


**FIGURE 6** Effects of middle domain residues on activities of ClpL. A, Relative ATPase activities of ClpL and its middle domain (MD) mutants. Results from biological triplicates are shown. B, Relative holdase/disaggregase activities of ClpL and its MD mutants. Turbidity of luciferase was monitored at 575 nm at designated time intervals. Each mutant is colored differently. C, Refolding of chemically denatured luciferase by ClpL and its MD mutants. Renaturation of firefly luciferase was monitored by measuring luminescence from refolded luciferase. Values are normalized to the percentage of luminescence of the ClpL-WT. Results from biological triplicates are shown. D, Relative refolding of heat-denatured GFP by ClpL and its MD mutants. Renaturation of GFP was monitored by measuring fluorescence from refolded GFP. Values are normalized to percentage of the ClpL-WT fluorescence. In all panels, statistical significance is represented as follows: \*,  $P \leq .05$ ; \*\*,  $P \leq .01$ ; and \*\*\*,  $P \leq .001$ ; NS, not significant.

of MDs relative to other domains of protomers. Multiple sequence alignment of the MDs of ClpL, ClpC, and ClpE orthologs reveal that many key residues in the MD interactions of ClpL including E348, F350, A353, and K357 are well conserved (Figure S8G).

The MDs of other AAA+ ATPases are reported to be equatorial (ClpB and Hsp104),<sup>26,62</sup> intermediate (ClpC),<sup>13</sup> and axial (dodecameric ClpC).<sup>21</sup> In terms of the angle that the MDs make in reference to the NBDs of an oligomer, the MDs of ClpL are almost perpendicular (Figure S9D). The

vertical positioning of the MD of ClpL becomes clear when compared to the positioning of the MDs of ClpC, ClpB, and Hsp104 when the NBD1s are superposed (Figure 5C-F). The MD of ClpC makes 56° angle with the MD of ClpL for the active conformation complexed with MecA (Figure 5C) and 51° angle for the repressed, inactive conformation (Figure 5D). The MDs of ClpB and its eukaryotic ortholog Hsp104 make a 75° angle with the MD of ClpL (Figure 5E and F). These analyses clearly demonstrate that the positioning of the MD of ClpL is quite different from that of the MDs of other phylogenetically related Clp proteins. The head-to-head interactions observed in the MDs of ClpL were also distinct from those of other Clp family proteins where the MD binds to their auxiliary co-chaperone proteins (Figure S9A). Multiple sequence alignment of the MDs from ClpL, ClpB, and Hsp104 shows some variability (Figure S9B). These results support that the MDs of ClpL are pivotal in ensuring the tetradecameric oligomeric state of ClpL.

### 3.6 | Tetradecameric ClpL is functionally active

It was previously reported that ClpB, an ortholog of ClpL, can exist as an inactive heptamer.<sup>20</sup> To investigate whether ClpL tetradecamer observed in the cryo-EM structures are functionally active, we performed activity assays such as ATPase, holdase/disaggregase, and refoldase ones (Figure 6). An M-domain deletion mutant  $\Delta$ 339-356 and single mutants showed no significant reduction in ATPase activities (Figure 6A), reflecting the established notion that ATPase activity is mediated by NBDs, not by MDs. Mutations in the MD of ClpL deteriorated holdase/disaggregase activity (Figure 6B), corroborating that integrity of the tetradecameric oligomeric state is critical in ensuring the activity. A triple mutant at the interface of MDs, D349A/F350A/E351A, exhibited the most severe reduction in holdase/disaggregase activity of ClpL, further supporting the importance of these residues and thereby of tetradecameric arrangement. Chaperone activity of ClpL, probed by refolding of chemically denatured luciferase and heat-denatured GFP, sheds light on the mechanistic aspect of ClpL chaperone. Refolding of luciferase was negatively affected by mutations in the MD (Figure 6C and D). Notably, mutations in the bottom tip of MD such as D349A, F350A, F350A/L354A, and D349A/F350A/E351A showed the most drastic reduction in the chaperone activity. In contrast, refolding of GFP was less deteriorated by aforementioned mutants, implicating that the chaperone activity of ClpL may differ depending on substrate polypeptides. Collectively, these activity assay results establish that the tetradecameric ClpL is functionally active.

## 4 | DISCUSSION

Functional AAA+ ATPases have been assumed to be either hexameric or dodecameric oligomers. Here we report a functional tetradecameric AAA+ ATPase structure of ClpL. Combined by cryo-EM, SAXS, and biochemical data, we demonstrate that the tetradecameric ClpL is a functionally active ATPase. The previously reported, inactive heptameric ClpB forms in the absence of salt and ATP.<sup>20</sup> Since ATP apparently stabilizes hexameric ClpB,<sup>63</sup> the heptameric ClpB is likely to be an inactive oligomer. However, ClpL forms tetradecamers only upon binding to ATP (Figure 1). Other instances of heptameric ATPases include HslU<sup>64</sup> and RuvB.<sup>65</sup> In both cases, the heptameric oligomer state represents functionally inactive states, either in the absence of ATP for HslU or of DNA for RuvB. ClpP, belonging to the same Clp family, functions as a heptamer, but the structure and function differ from those of ClpL (Figure S10).<sup>66-68</sup> Heptameric ClpP forms a two-component protease complex with hexameric ClpX or ClpA for the chaperone. In contrast, ClpL is an AAA+ chaperone that can function without any auxiliary factor. A recent study reported a heptameric assembly of yeast Bcs1, an AAA+ ATPase, involved in the transport of folded proteins.<sup>69</sup> However, Bcs1 has a domain architecture different from that of ClpL. To the best of our knowledge, this is the first case where an AAA+ ATPase is active as a heptamer-based oligomer.

Our analyses on residues in the protomer interfaces shed light on determinants for heptameric ring formation for HSP100 and AAA+ ATPases. Non-conserved residues seem to be critical in forming a heptameric assembly, while conserved residues apparently participate in hexameric assembly (Figure 4). The relative positioning of residues in the NBD1 and NBD2 interfaces may contribute to the distinction between heptameric and hexameric assemblies. The heptameric assembly shows the clockwise rotation of the NBD1 interface residue to the NBD2 interface residue, while the hexameric assembly exhibits the counter-clockwise rotation (Figure S7). The chamber volume analysis also hints on the requirement of heptameric assembly for ClpL. The heptameric ring of ClpL contributes to only about half the chamber volume of hexameric ClpC and ClpB, implicating that the two-layered tetradecameric assembly of ClpL might warrant functionality as a chaperone (Figure 3C). It requires further investigation whether these features found in the tetradecameric ClpL structure can be extended beyond the HSP100 family to AAA+ ATPases in general.

The position of the MD relative to the NBDs has been implicated in different functional states of AAA+ ATPases. Lateral MD is associated with active states, exemplified in ClpB,<sup>60</sup> while vertical MD with inactive state as shown in the case of “repressed” ClpC.<sup>21</sup> The MD of ClpL assumes the most

vertical position among known ring-type AAA+ ATPases (Figure S9A), but this position is obviously correlated with the functionally active state.

Functional tetradecameric ClpL labels it as a unique ring-type ATPase. While most AAA+ ATPases are hexamer-based oligomers, many proteins working in conjunction with AAA+ ATPases feature non-hexameric oligomeric states. For instance, ClpX, a bacterial protease working with ClpB and other bacterial chaperones, functions as a heptamer. GroEL-GroES chaperone complex shows the heptamer-based architecture. It seems that ClpL is positioned between heptamer-based chaperones and proteases and hexamer-based canonical AAA+ ATPases, rendering ClpL in a unique position in lieu of oligomeric structure. Such uniqueness of tetradecameric ClpL is also reflected in the oligomeric interfaces: some residues are specific to ClpL, while others are involved in hexameric orthologs (Figure 4A and Figure S5). Phylogenetic analysis of ClpL with its orthologs,<sup>32</sup> combined with multiple sequence alignments, implicates that tetradecameric arrangement may represent a subgroup of AAA+ ATPases (Figure S8G). For instance, ClpE from *Leptotrichia wadei* is closest to ClpL in the phylogeny and shows 82% sequence identity. Sequence alignment shows that key residues in protomer interface and MD are well conserved, corroborating the idea that more AAA+ ATPases may exist as non-hexameric oligomers, including tetradecamers.

## ACKNOWLEDGEMENTS

We thank Dr. Sang-Sang Park for his contribution in the early stage of this work, staff members at the beamline 4C of Pohang Acceleratory Laboratory and Dr. Donghyuk Shin for technical assistance in SAXS data collection and processing, Drs. Sunghwan Kim, Tae Ho Jang, and Eunmi Hong at Daegu Gyeongbuk Advanced Medical Industry Promotion Foundation and Mr. Jin-Ku Park at Mokpo National University for technical assistance in AUC data collection and processing, and Korea Research Environment Open Network/Global Ring Network for Advanced Applications Development (KREONET/GLORIAD) and Global Science experimental Data hub Center (GSDC) at Korea Institute of Science and Technology Information (KISTI) for computing resources and technical support. This work was supported by the Basic Science Research Program (NRF-2018R1A2B6004367) and the Science Research Center Program (NRF-2017R1A5A1014560) through the National Research Foundation of Korea (NRF) grants and the Next-Generation BioGreen 21 program (PJ01367602) through the Rural Development Agency to S. Lee, and by the Institute of Basic Science (IBS-R030-C1) to S.-G. Lee and H. Kim.

## AUTHOR CONTRIBUTIONS

G. Kim performed most experiments including cryo-EM ones and analyzed results; S.-G. Lee and H. Kim performed cryo-EM experiments and analyzed results; S. Han analyzed

cryo-EM data; J. Jung purified samples; H. Jeong and J.-K. Hyun collected cryo-EM data; D. Rhee analyzed activity assay results; S. Lee designed and supervised research; and G. Kim, S.-G. Lee, H. Kim, and S. Lee wrote the manuscript with inputs from all authors.

## REFERENCES

1. Doyle SM, Genest O, Wickner S. Protein rescue from aggregates by powerful molecular chaperone machines. *Nat Rev Mol Cell Biol.* 2013;14:617-629. <https://doi.org/10.1038/nrm3660>
2. Hayer-Hartl MK, Martin J, Hartl FU. Asymmetrical interaction of GroEL and GroES in the ATPase cycle of assisted protein folding. *Science.* 1995;269:836-841. <https://doi.org/10.1126/science.7638601>
3. Todd MJ, Viitanen PV, Lorimer GH. Dynamics of the chaperonin ATPase cycle: implications for facilitated protein folding. *Science.* 1994;265:659-666. <https://doi.org/10.1126/science.7913555>
4. Thomas JG, Baneyx F. ClpB and HtpG facilitate de novo protein folding in stressed *Escherichia coli* cells. *Mol Microbiol.* 2000;36:1360-1370.
5. Hartl FU, Bracher A, Hayer-Hartl M. Molecular chaperones in protein folding and proteostasis. *Nature.* 2011;475:324-332. <https://doi.org/10.1038/nature10317>
6. Corrales FJ, Fersht AR. Toward a mechanism for GroEL-GroES chaperone activity: an ATPase-gated and -pulsed folding and annealing cage. *Proc Natl Acad Sci USA.* 1996;93:4509-4512. <https://doi.org/10.1073/pnas.93.9.4509>
7. Puchades C, Sandate CR, Lander GC. The molecular principles governing the activity and functional diversity of AAA+ proteins. *Nat Rev Mol Cell Biol.* 2020;21:43-58. <https://doi.org/10.1038/s41580-019-0183-6>
8. Zolkiewski M, Zhang T, Nagy M. Aggregate reactivation mediated by the Hsp100 chaperones. *Arch Biochem Biophys.* 2012;520:1-6. <https://doi.org/10.1016/j.abb.2012.01.012>
9. Saibil H. Chaperone machines for protein folding, unfolding and disaggregation. *Nat Rev Mol Cell Biol.* 2013;14:630-642. <https://doi.org/10.1038/nrm3658>
10. Duran EC, Weaver CL, Lucius AL. Comparative analysis of the structure and function of AAA+ motors ClpA, ClpB, and Hsp104: common threads and disparate functions. *Front Mol Biosci.* 2017;4:54. <https://doi.org/10.3389/fmolb.2017.00054>
11. Ogura T, Wilkinson AJ. AAA+ superfamily ATPases: common structure-diverse function. *Genes Cells.* 2001;6:575-597. <https://doi.org/10.1046/j.1365-2443.2001.00447.x>
12. Doyle SM, Wickner S. Hsp104 and ClpB: protein disaggregating machines. *Trends Biochem Sci.* 2009;34:40-48. <https://doi.org/10.1016/j.tibs.2008.09.010>
13. Wang F, Mei Z, Qi Y, et al. Structure and mechanism of the hexameric Meca-ClpC molecular machine. *Nature.* 2011;471:331-335. <https://doi.org/10.1038/nature09780>
14. Kirstein J, Moliere N, Dougan DA, Turgay K. Adapting the machine: adaptor proteins for Hsp100/Clp and AAA+ proteases. *Nat Rev Microbiol.* 2009;7:589-599. <https://doi.org/10.1038/nrmicro2185>
15. Sweeny EA, Shorter J. Mechanistic and structural insights into the prion-disaggregase activity of Hsp104. *J Mol Biol.* 2016;428:1870-1885. <https://doi.org/10.1016/j.jmb.2015.11.016>
16. Zheng J, Wu Y, Lin Z, et al. ClpP participates in stress tolerance, biofilm formation, antimicrobial tolerance, and virulence of *Enterococcus faecalis*. *BMC Microbiol.* 2020;20:30. <https://doi.org/10.1186/s12866-020-1719-9>

17. Lopez KE, Rizo AN, Tse E, et al. Conformational plasticity of the ClpAP AAA+ protease couples protein unfolding and proteolysis. *Nat Struct Mol Biol.* 2020;27:406-416. <https://doi.org/10.1038/s41594-020-0409-5>
18. Zolkiewski M. ClpB cooperates with DnaK, DnaJ, and GrpE in suppressing protein aggregation. A novel multi-chaperone system from *Escherichia coli*. *J Biol Chem.* 1999;274:28083-28086.
19. Lee S, Sowa ME, Watanabe Y-H, et al. The structure of ClpB: a molecular chaperone that rescues proteins from an aggregated state. *Cell.* 2003;115:229-240.
20. Kim KI, Cheong GW, Park SC, et al. Heptameric ring structure of the heat-shock protein ClpB, a protein-activated ATPase in *Escherichia coli*. *J Mol Biol.* 2000;303:655-666. <https://doi.org/10.1006/jmbi.2000.4165>
21. Carroni M, Franke KB, Maurer M, et al. Regulatory coiled-coil domains promote head-to-head assemblies of AAA+ chaperones essential for tunable activity control. *Elife.* 2017;6:e30120. <https://doi.org/10.7554/eLife.30120>
22. Biter AB, Lee S, Sung N, Tsai FT. Structural basis for intersubunit signaling in a protein disaggregating machine. *Proc Natl Acad Sci USA.* 2012;109:12515-12520. <https://doi.org/10.1073/pnas.1207040109>
23. Yamasaki T, Oohata Y, Nakamura T, Watanabe YH. Analysis of the cooperative ATPase cycle of the AAA+ chaperone ClpB from *Thermus thermophilus* by using ordered heterohexamers with an alternating subunit arrangement. *J Biol Chem.* 2015;290:9789-9800. <https://doi.org/10.1074/jbc.M114.617696>
24. Li T, Weaver CL, Lin J, Duran EC, Miller JM, Lucius AL. *Escherichia coli* ClpB is a non-processive polypeptide translocase. *Biochem J.* 2015;470:39-52. <https://doi.org/10.1042/BJ20141457>
25. Kedzierska S, Akoef V, Barnett ME, Zolkiewski M. Structure and function of the middle domain of ClpB from *Escherichia coli*. *Biochemistry.* 2003;42:14242-14248. <https://doi.org/10.1021/bi035573d>
26. Lee S, Sowa ME, Choi JM, Tsai FT. The ClpB/Hsp104 molecular chaperone—a protein disaggregating machine. *J Struct Biol.* 2004;146:99-105. <https://doi.org/10.1016/j.jsb.2003.11.016>
27. Yokom AL, Gates SN, Jackrel ME, et al. Spiral architecture of the Hsp104 disaggregase reveals the basis for polypeptide translocation. *Nat Struct Mol Biol.* 2016;23:830-837. <https://doi.org/10.1038/nsmb.3277>
28. Gates SN, Yokom AL, Lin JiaBei, et al. Ratchet-like polypeptide translocation mechanism of the AAA+ disaggregase Hsp104. *Science.* 2017;357:273-279. <https://doi.org/10.1126/science.aan1052>
29. Deville C, Carroni M, Franke KB, et al. Structural pathway of regulated substrate transfer and threading through an Hsp100 disaggregase. *Sci Adv.* 2017;3:e1701726. <https://doi.org/10.1126/sciadv.1701726>
30. Rizo AN, Lin JiaBei, Gates SN, et al. Structural basis for substrate gripping and translocation by the ClpB AAA+ disaggregase. *Nat Commun.* 2019;10:2393. <https://doi.org/10.1038/s41467-019-10150-y>
31. Shorter J, Southworth DR. Spiraling in control: structures and mechanisms of the Hsp104 disaggregase. *Cold Spring Harb Perspect Biol.* 2019;11(8):a034033. <https://doi.org/10.1101/cshperspect.a034033>
32. Miller JM, Chaudhary H, Marsee JD. Phylogenetic analysis predicts structural divergence for proteobacterial ClpC proteins. *J Struct Biol.* 2018;201:52-62. <https://doi.org/10.1016/j.jsb.2017.11.003>
33. Park S-S, Kwon H-Y, Tran T-H, et al. ClpL is a chaperone without auxiliary factors. *FEBS J.* 2015;282:1352-1367. <https://doi.org/10.1111/febs.13228>
34. Zhang X, Wigley DB. The “glutamate switch” provides a link between ATPase activity and ligand binding in AAA+ proteins. *Nat Struct Mol Biol.* 2008;15:1223-1227. <https://doi.org/10.1038/nsmb.1501>
35. Schuck P, Gillis RB, Besong TMD, et al. SEDFIT-MSTAR: molecular weight and molecular weight distribution analysis of polymers by sedimentation equilibrium in the ultracentrifuge. *Analyst.* 2014;139:79-92. <https://doi.org/10.1039/c3an01507f>
36. Laue T, Shah B, Ridgeway T, En PS. Analytical ultracentrifugation in biochemistry & polymer science. In: Harding SE, Horton HC, Rowe AJ, eds. London: Royal Society of Chemistry; 1992:90-125.
37. Scheres SH. RELION: implementation of a Bayesian approach to cryo-EM structure determination. *J Struct Biol.* 2012;180:519-530. <https://doi.org/10.1016/j.jsb.2012.09.006>
38. Li X, Mooney P, Zheng S, et al. Electron counting and beam-induced motion correction enable near-atomic-resolution single-particle cryo-EM. *Nat Methods.* 2013;10:584-590. <https://doi.org/10.1038/nmeth.2472>
39. Rohou A, Grigorieff N. CTFIND4: fast and accurate defocus estimation from electron micrographs. *J Struct Biol.* 2015;192:216-221. <https://doi.org/10.1016/j.jsb.2015.08.008>
40. Heymann JB, Belnap DM. Bsoft: image processing and molecular modeling for electron microscopy. *J Struct Biol.* 2007;157:3-18. <https://doi.org/10.1016/j.jsb.2006.06.006>
41. Grant T, Rohou A, Grigorieff N. cisTEM, user-friendly software for single-particle image processing. *Elife.* 2018;7:e35383. <https://doi.org/10.7554/eLife.35383>
42. Pettersen EF, Goddard TD, Huang CC, et al. UCSF Chimera—a visualization system for exploratory research and analysis. *J Comput Chem.* 2004;25:1605-1612. <https://doi.org/10.1002/jcc.20084>
43. Emsley P, Cowtan K. Coot: model-building tools for molecular graphics. *Acta Crystallogr D Biol Crystallogr.* 2004;60:2126-2132. <https://doi.org/10.1107/S0907444904019158>
44. Adams PD, Afonine PV, Bunkoczi G, et al. PHENIX: a comprehensive Python-based system for macromolecular structure solution. *Acta Crystallogr D Biol Crystallogr.* 2010;66:213-221. <https://doi.org/10.1107/S0907444909052925>
45. Wang RY, Song Y, Barad BA, Cheng Y, Fraser JS, DiMaio F. Automated structure refinement of macromolecular assemblies from cryo-EM maps using Rosetta. *Elife.* 2016;5:e17219. <https://doi.org/10.7554/eLife.17219>
46. Dmitri S. Determination of the regularization parameter in indirect-transform methods using perceptual criteria. *J Appl Crystallogr.* 1992;25:495-503.
47. Daniel F, Petoukhov M, Konarev P, et al. ATSAS 2.8: a comprehensive data analysis suite for small-angle scattering from macromolecular solutions. *J Appl Crystallogr.* 2017;50:1212-1225. <https://doi.org/10.1107/S1600576717007786>
48. Daniel F, Dmitri S. DAMMIF, a program for rapid ab-initio shape determination in small-angle scattering. *J Appl Crystallogr.* 2009;42:342-346. <https://doi.org/10.1107/S0021889809000338>
49. Vladimir VV, Dmitri S. Uniqueness of ab initio shape determination in small-angle scattering. *J Appl Crystallogr.* 2003;36:860-864. <https://doi.org/10.1107/S0021889803000268>
50. Dmitri S. Restoring low resolution structure of biological macromolecules from solution scattering using simulated annealing.

- Biophys J.* 1999;76:2879-2886. [https://doi.org/10.1016/S0006-3495\(99\)77443-6](https://doi.org/10.1016/S0006-3495(99)77443-6)
51. Mikhail K, Dimitri S. Automated matching of high- and low-resolution structural models. *J Appl Crystallogr.* 2001;34:33-41.
  52. Saeed IA, Ashraf SS. Denaturation studies reveal significant differences between GFP and blue fluorescent protein. *Int J Biol Macromol.* 2009;45:236-241. <https://doi.org/10.1016/j.ijbmac.2009.05.010>
  53. Liu J, Mei Z, Li N, et al. Structural dynamics of the MecA-ClpC complex: a type II AAA+ protein unfolding machine. *J Biol Chem.* 2013;288:17597-17608. <https://doi.org/10.1074/jbc.M113.458752>
  54. Zolkiewski M, Kessel M, Ginsburg A, Maurizi MR. Nucleotide-dependent oligomerization of ClpB from *Escherichia coli*. *Protein Sci.* 1999;8:1899-1903. <https://doi.org/10.1110/ps.8.9.1899>
  55. Shiau AK, Harris SF, Southworth DR, Agard DA. Structural analysis of *E coli* hsp90 reveals dramatic nucleotide-dependent conformational rearrangements. *Cell.* 2006;127:329-340. <https://doi.org/10.1016/j.cell.2006.09.027>
  56. Ewens CA, Su M, Zhao L, Nano N, Houry WA, Southworth DR. Architecture and nucleotide-dependent conformational changes of the Rvb1-Rvb2 AAA+ complex revealed by cryoelectron microscopy. *Structure.* 2016;24:657-666. <https://doi.org/10.1016/j.str.2016.03.018>
  57. Yu H, Lupoli TJ, Kovach A, et al. ATP hydrolysis-coupled peptide translocation mechanism of *Mycobacterium tuberculosis* ClpB. *Proc Natl Acad Sci USA.* 2018;115:E9560-E9569. <https://doi.org/10.1073/pnas.1810648115>
  58. Lipińska N, Ziętkiewicz S, Sobczak A, et al. Disruption of ionic interactions between the nucleotide binding domain 1 (NBD1) and middle (M) domain in Hsp100 disaggregase unleashes toxic hyperactivity and partial independence from Hsp70. *J Biol Chem.* 2013;288:2857-2869. <https://doi.org/10.1074/jbc.M112.387589>
  59. DeSantis ME, Sweeny EA, Snead D, et al. Conserved distal loop residues in the Hsp104 and ClpB middle domain contact nucleotide-binding domain 2 and enable Hsp70-dependent protein disaggregation. *J Biol Chem.* 2014;289:848-867. <https://doi.org/10.1074/jbc.M113.520759>
  60. Carroni M, Kummer E, Oguchi Y, et al. Head-to-tail interactions of the coiled-coil domains regulate ClpB activity and cooperation with Hsp70 in protein disaggregation. *Elife.* 2014;3:e02481. <https://doi.org/10.7554/eLife.02481>
  61. Rambo RP, Tainer JA. Characterizing flexible and intrinsically unstructured biological macromolecules by SAS using the Porod-Debye law. *Biopolymers.* 2011;95:559-571. <https://doi.org/10.1002/bip.21638>
  62. Barnett ME, Zolkiewska A, Zolkiewski M. Structure and activity of ClpB from *Escherichia coli*. Role of the amino- and -carboxyl-terminal domains. *J Biol Chem.* 2000;275:37565-37571. <https://doi.org/10.1074/jbc.M005211200>
  63. Akoev V, Gogol EP, Barnett ME, Zolkiewski M. Nucleotide-induced switch in oligomerization of the AAA+ ATPase ClpB. *Protein Sci.* 2004;13:567-574. <https://doi.org/10.1110/ps.03422604>
  64. Rohrwild M, Pfeifer G, Santarius U, et al. The ATP-dependent HslVU protease from *Escherichia coli* is a four-ring structure resembling the proteasome. *Nat Struct Mol Biol.* 1997;4:133-139.
  65. Miyata T, Yamada K, Iwasaki H, Shinagawa H, Morikawa K, Mayanagi K. Two different oligomeric states of the RuvB branch migration motor protein as revealed by electron microscopy. *J Struct Biol.* 2000;131:83-89. <https://doi.org/10.1006/jsbi.2000.4290>
  66. Ishikawa T, Beuron F, Kessel M, Wickner S, Maurizi MR, Steven AC. Translocation pathway of protein substrates in ClpAP protease. *Proc Natl Acad Sci USA.* 2001;98:4328-4333. <https://doi.org/10.1073/pnas.081543698>
  67. Ripstein ZA, Vahidi S, Houry WA, Rubinstein JL, Kay LE. A processive rotary mechanism couples substrate unfolding and proteolysis in the ClpXP degradation machinery. *Elife.* 2020;9: <https://doi.org/10.7554/eLife.52158>
  68. Gatsogiannis C, Balogh D, Merino F, Sieber SA, Raunser S. Cryo-EM structure of the ClpXP protein degradation machinery. *Nat Struct Mol Biol.* 2019;26:946-954. <https://doi.org/10.1038/s41594-019-0304-0>
  69. Kater L, Wagener N, Berninghausen O, Becker T, Neupert W, Beckmann R. Structure of the Bcs1 AAA-ATPase suggests an airlock-like translocation mechanism for folded proteins. *Nat Struct Mol Biol.* 2020;27(2):142-149. <https://doi.org/10.1038/s41594-019-0364-1>
  70. Masood TB, Sandhya S, Chandra N, Natarajan V. CHEXVIS: a tool for molecular channel extraction and visualization. *BMC Bioinformatics.* 2015;16:119. <https://doi.org/10.1186/s12859-015-0545-9>

## SUPPORTING INFORMATION

Additional Supporting Information may be found online in the Supporting Information section.

**How to cite this article:** Kim G, Lee S-G, Han S, et al. ClpL is a functionally active tetradecameric AAA+ chaperone, distinct from hexameric/dodecameric ones. *The FASEB Journal.* 2020;34:14353–14370. <https://doi.org/10.1096/fj.202000843R>